Acta Neuropathologica Communications

RESEARCH Open Access

Distinct subcellular localization of tau and alpha-synuclein in lewy body disease

D. Luke Fischer[1*], Marissa Menard[1], Omar Z. Abdelaziz[1], Nicholas M. Kanaan[3], Virginia G. Cobbs[1], Richard E. Kennedy[4], Geidy E. Serrano[2], Thomas G. Beach[2] and Laura A. Volpicelli-Daley[1*]

Abstract

Lewy bodies and neurofibrillary tangles, composed of α-synuclein (α-syn) and tau, respectively, often are found together in the same brain and correlate with worsening cognition. Human postmortem studies show colocalization of α-syn and tau occurs in Lewy bodies, but with limited effort to quantify colocalization. In this study, postmortem middle temporal gyrus tissue from decedents ($n=9$) without temporal lobe disease (control) or with Lewy body disease (LBD) was immunofluorescently labeled with antibodies to phosphorylated α-syn (p-α-syn), tau phosphorylated at Ser202/Thr205 (p-tau), or exposure of tau's phosphatase-activating domain (PAD-tau) as a marker of early tau aggregates. Immunofluorescence for major-histocompatibility complex class 2 (MHCII) and ionized calcium binding adaptor molecule 1 (Iba1) also was performed because inflammation is an additional pathological hallmark of LBDs, and they were a positive control for two markers known to colocalize. The abundance of p-α-syn, p-tau, and MHCII was significantly associated with diagnosis of LBD. Quantification of colocalization showed that MHCII and Iba1 colocalized, demonstrating activated immune cells are mostly microglia. However, p-α-syn rarely colocalized with p-tau or PAD-tau, although the overlap of p-α-syn with PAD-tau was significantly associated with LBD. In the rare cases pathologic α-syn and pathologic tau were found in the same Lewy body or Lewy neurite, tau appeared to surround α-syn but did not colocalize within the same structure. The relationship between tau and α-syn copathology is important for explaining clinical symptoms, severity, and progression, but there is no evidence for frequent, direct protein-protein interactions in the middle temporal gyrus.

Keywords Tau, Alpha-synuclein, Lewy body, Neurofibrillary tangle, Copathology

Introduction

Dementia with Lewy Bodies (DLB), Parkinson's disease (PD) and PD dementia (PDD) are neurodegenerative syndromes that are characterized neuropathologically by Lewy body disease (LBD), including Lewy bodies in neuronal somata and Lewy neurites in axons or dendrites. Intraneuronal aggregates of tau called neurofibrillary tangles (NFTs) classically are associated with Alzheimer's disease (AD), yet NFTs often are observed with LBD as well [40]. PDD patients have a higher burden of NFTs in the cortex compared to PD patients without dementia, and cortical tau aggregates correlate with cognitive impairment severity [15, 21, 22]. Mouse models of LBD

*Correspondence:
D. Luke Fischer
david.fischer2@ucsf.edu
Laura A. Volpicelli-Daley
lvolpicellidaley@uabmc.edu
[1]Center for Neurodegeneration and Experimental Therapeutics, Department of Neurology, University of Alabama at Birmingham, Birmingham, AL, USA
[2]Banner Sun Health Research Institute, Sun City, AZ, USA
[3]Department of Translational Neuroscience, College of Human Medicine, Michigan State University, Grand Rapids, MI, USA
[4]Department of Medicine, University of Alabama at Birmingham, Birmingham, AL, USA

implicate an α-syn-tau interaction. In mice overexpressing A53T mutant human α-syn, knocking out tau or using antibodies targeting oligomeric tau reverses memory impairments [19, 39]. Thus, the presence of both Lewy and tau pathology may contribute to cognitive symptoms from LBD.

Endogenous tau and α-synuclein colocalize and associate in neurons [42], suggesting that co-pathology may arise from synergistic interactions. Indeed, in vitro experiments show that tau's microtubule binding domain also binds the C-terminus of α-syn, resulting in the fibrillization and aggregation of both proteins [17, 20]. In addition, human postmortem studies report colocalization between tau and synuclein using various antibody combinations. LBD colocalizes with tau in brainstem Sect. [2], hippocampus [3], entorhinal cortex [23], frontal cortex [38], amygdala [37, 43], and olfactory bulb [18]. One study quantified the number of double-positive neurons across hippocampal structures and determined the subiculum and pre-CA1 neurons had the highest proportion for double-positivity with a range of 1–13% across 5 subjects, as assessed by examining neuronal somata [24]. In another study that focused on brainstem Lewy bodies, as many as a third of Lewy bodies in the medulla were immunoreactive for phosphorylated tau, but a relationship between tau and α-syn immunoreactivity within abundant Lewy neurites has not been examined [25]. In addition, many of the studies showing overlap of α-syn and tau pathology are qualitative or relied on counting colocalization by eye in single images rather than quantifying colocalization over a larger area within the tissue.

Investigating overlap of pathologic α-syn and tau in structures including neurites is important because synaptic and axonal dysfunction are earlier pathophysiologic events in LBD than the formation of Lewy bodies, and cortical and limbic regions affected by α-synucleinopathy show more abundant Lewy neurites than Lewy bodies. We examined postmortem middle temporal gyrus cortex from human brains with confirmed LBD using immunofluorescence and confocal microscopy. We first quantified the degree of abnormal forms of α-syn and tau as well as immunologic markers for this region, showing an association of disease markers with the neuropathological diagnosis of LBD, demonstrating these cases recapitulate prior findings from the literature. We then measured colocalization of pathologic α-syn with phosphorylated tau, and an early pathologic form of tau. Contrary to expectations from the literature, colocalization between these proteins in middle temporal gyrus neocortex is a rare event and does not support the hypothesis that tau and α-syn pathologies extensively interact intracellularly at a protein-protein level as a pathophysiologic driver in mixed degenerative disease.

Materials and methods

Human brain tissue

Deidentified postmortem brain tissue was obtained from the Banner Sun Health Research Institute Brain and Body Donation Program in Sun City, Arizona [6]. Subjects undergo annual cognitive evaluations prior to death. Neuropathologic examination was described previously [6], and includes the Unified Staging System for Lewy Body Disorders [1]. Cases were selected for the presence of neocortical (stage IV) LBD that included middle temporal gyrus involvement ($n = 6$) along with three control cases ($n = 3$). Formalin-fixed, free-floating, temporal lobe sections of 40 µm thickness were used for immunofluorescence-based analyses.

Immunohistochemistry

Free-floating sections were rinsed extensively with phosphate buffered saline (PBS) and blocked at room temperature with shaking for two hours using 5% normal donkey or goat serum and 0.1% Triton X-100 in PBS for all antibodies except MHCII and Iba1 where 5% normal in blocking and antibody diluent solutions. Tissues were then incubated overnight at 4 °C with primary antibodies diluted in their respective blocking buffer with Triton-X-100 omitted for the MHCII/Iba1 condition. Primary antibodies for phosphorylated (pS129) α-syn (MJF-R13, hereafter "R13", Abcam ab168381, RRID: AB_2728613, 1:1000); and for phosphorylated tau (AT8 for pS202/pT205/pS208, Fisher MN1020, RRID: AB_223647, 1:1000); the phosphatase activating domain (PAD) of tau (TNT1, Kanaan Lab, RRID: AB_2736930, 1:30,000; [12, 13, 26]), major histocompatibility complex class II (MHCII, Invitrogen 14-9956-82, RRID: AB_468639, 1:750), ionized calcium binding adaptor molecule 1 (Iba1, Wako 019-19741, RRID: AB_839504, 1:1000), and vesicular glutamate transporter 1 (vGLUT1, Synaptic Systems 135304, RRID: AB_887878, 1:1000) were used in combinations as specified. After washes, sections were incubated with secondary antibodies diluted in blocking buffer at room temperature with gentle shaking for two hours. Combinations of the following secondary antibodies from ThermoFisher were used: goat anti-mouse IgG1 Alexa Fluor 488 (A-21121, RRID: AB_2535764, 1:500), goat anti-rabbit IgG Alexa Fluor 555 (RRID: AB_2535850, 1:500), goat anti-guinea pig IgG Alexa Fluor 647 (A-21450, RRID: AB_2535867, 1:500), goat anti-mouse IgM Alexa Fluor 555 (A-21426, RRID: AB_2535847, 1:500), goat anti-rabbit IgG Alexa Fluor 647 (A-21245, RRID: AB_2535813, 1:500), and goat anti-mouse IgG Alexa Fluor 488 (A-11001, RRID: AB_2534069, 1:500). p-α-Syn and tau-stained sections were washed and treated with 1% Sudan Black B for 2–3 min followed by washes, whereas MHCII and Iba1 stained sections were treated with 10 mM copper

sulfate and 50 mM ammonium sulfate solution at 4 °C for 15 min. After washing, sections were mounted using the free-floating technique on adhesion Superfrost Plus microscope slides, air dried briefly, and mounted using Prolong Gold antifade mountant (Fisher P36934). Of note, every immunohistochemical experiment included a primary delete (i.e., no primary antibodies used) for each subject that was processed in parallel. Of note, no additional antigen retrieval steps were used, and proteinase K was not in any step to remove normal α-syn.

Imaging and deconvolution

Confocal imaging was performed on a Nikon Ti2 confocal microscope with 10X, 40X-oil (NA 1.3), and 60X-oil (NA 1.4) immersion objectives. For each set of antibodies, the same laser intensity, gain, pinhole diameter and offset was used across all cases. Z-stacks were acquired using a 0.1 µm step size for a minimum of 3 µm total thickness. Only portions of the gray matter were imaged; the z-stacks were obtained to avoid the outer edges of the tissue, starting from one side of tissue and moving in a semi-random, consistent way across the cortex so optical sections were non-overlapping. All images underwent deconvolution using NIS-Elements using the Richardson-Lucy algorithm for 20 iterations on a Nikon Elements analysis workstation at the UAB High Resolution Imaging Facility.

Percent area occupied analysis

To determine the abundance of R13, AT8, TNT1, MHCII and Iba1 positive immunofluorescent signal, the area fraction measurement in FIJI was analyzed for each of the 10 z-stacks captured for each case using the original ND2 files. The resolution was 2048 × 2048 for AT8/R13 and 1024 × 1024 for MHCII/Iba1 and TNT1/R13 analyses. A researcher blinded to diagnosis of each case performed the quantitation. The z-stacks were converted to 8-bit images and collapsed into maximum projection images prior to area fraction analysis. After reviewing each of the thresholding filters using the pre-packaged mask feature, the "triangle" mask was found to be the most accurate in detecting the true fluorescent signal present in each image for the α-syn/tau-stained sections, whereas the "default" mask was chosen for the MHCII/Iba1 images. Of note, the prepackaged mask feature automatically determines the acceptable threshold for each image which determines the percent area occupied in FIJI. For the vast majority of the images the auto-threshold provided by the mask was a faithful representation of what was seen in the image by the blinded researcher; however, when the mask clearly was over- or under-capturing signal, the threshold was manually adjusted using the histogram to provide a more accurate representation of the fluorescent signal seen. The values are reported in percentage of area occupied by the fluorescent pixels falling within the defined threshold for each image.

Colocalization analysis

For determining the degree of colocalization of two immunofluorescent signals, a total of 10 non-overlapping z-stacks per case were acquired at 60X for synuclein/tau analysis and 40X for MHCII/Iba1 analysis by a researcher blinded to diagnosis of each case. As above, each z-stack location was chosen within cortical gray matter. Stacks of images were loaded and analyzed together in FIJI using the JaCOP feature to generate the thresholded Mander's colocalization coefficients [8].

Statistical analyses

Two-sample t-tests and Fisher's exact tests were used to compare demographic and disease characteristics between groups (control or LBD). Mixed effects models (covariance pattern models) [9] were used to examine differences in colocalization coefficients between groups while accounting for repeated measures with 10 confocal frames captured for each case. A compound symmetric covariance structure was used to model the correlation among measurements on the same subject. Statistical significance was based on the t-test for the group (control vs. LBD) variable, using a Satterthwaite approximation for the degrees of freedom. All analyses were performed using the *lme4* package [5], version 1.1–34, in R (R Core Team 2022) version 4.2.1.

Results

Subject demographics

Brain tissue was derived from subjects with the presence or absence (controls) of LBD. Subject demographics are displayed in Table 1. Two measures were not recorded for some controls for logistical reasons. There were no significant differences in expiration date, sex, post-mortem interval, PD diagnosis, vascular AD diagnosis, APOE genotype, or Braak AD stage. There were significant differences in AD diagnosis, DLB diagnosis, and Unified Lewy Body stage.

Pathologic α-syn burden in the middle temporal gyrus of control and LBD cases

The R13 antibody against phospho-serine-129 (p-α-syn) was used to examine the degree of aberrant α-syn, regardless of whether it showed classic LBD morphological characteristics or earlier changes, in the middle temporal gyrus [7, 10]. Immunofluorescence was also performed for the synaptic marker, vGLUT1 so the localization of p-α-syn could be visualized relative to neuropil throughout the cortex. It is important to note that proteinase K was not included in our immunofluorescence protocol, unlike other pathologic studies which use it to

Table 1 Subject characteristics. Summary of neuropathologic assessments. *N=1. A dash indicates not enough data were available to make a comparison

	Control	LBD	*p* value
n	3	6	
Expired age (years+/-SEM)	76.3 (11.8)	74.3 (6.65)	0.81
Sex = female %	2 (66.7%)	3 (50%)	1.00
Postmortem interval (hours)	2.22 (0.26)*	2.71 (0.57)	0.12
Last MMSE test score	27.0 (0.0)*	3.33 (3.56)	-
Motor UPDRS score off	9.0(0.0)	44.0 (33.3)	-
Clinical diagnosis			
AD	0(0.0%)	4(66.7%)	-
parkinsonism	0(0.0%)	1(16.7%	-
DLB	0(0.0%)	1(16.7%)	-
Pathological Diagnosis			
AD	0 (0.0%)	6 (100%)	0.01
PD	0 (0.0%)	0 (0.0%)	-
DLB	0 (0.0%)	6 (100%)	0.02
Vascular AD	0 (0.0%)	1 (16.7%)	1.00
APOE			0.53
2/2	1 (33.3%)	0 (0.00%)	
3/3	0 (0.0%)	2 (33.3%)	
3/4	1 (33.3%)	3 (50.0%)	
4/4	1 (33.3%)	1 (16.7%)	
Braak NFT Stage			0.22
I	2 (66.7%)	0 (0.0%)	
III	1 (33.3%)	0 (0.0%)	
V	0 (0.0%)	2 (33.3%)	
VI	0 (0.0%)	4 (66.7%)	
Amyloid Plaque total, semiquantitative	5.58 (3.99)	14.5 (0.77)	0.06
Unified Lewy Body Stage			0.01
IV: Neocortical	0(0.0%)	6(100%)	

remove normal α-syn. In control cases, p-α-syn appeared as diffuse, dim immunofluorescence in the soma, likely reflecting physiologic, soluble p-α-syn (Fig. 1A) [34, 35]. In LBD cases, the majority of immunoreactivity appeared as bright puncta, and longer thread-like neurites, some of which were classical Lewy neurites with a larger, dystrophic morphology. Most immunoreactive neurites were independent but occasionally showed a denser network (Fig. 1A, case "DLB6"). Circular, dense Lewy bodies were rare but were present with brighter p-α-syn near the periphery of the inclusion. Overall, the average percent area occupied by p-α-syn in control cases was 2.2% (+/-0.14), and the average for LBD cases was 12.1% (+/-0.6). Note that case DLB 3 had a low percent occupied by p-α-syn such that the average was similar to controls. This case had a low MMSE score (0) and a relatively high UPDRS score (80). Analyses of the images show that the control cases do have low levels of small p-α-syn puncta, whereas DLB3 p-α-syn appeared as Lewy neurites (Online Resource 1). Overall, quantification of the percent area occupied by p-α-syn revealed a low level of p-α-syn in control cases with statistically significant increase in abundance in LBD cases ($t(7) = 2.6$, $p = 0.034$; Fig. 1B).

Pathologic tau burden in the middle temporal gyrus of control and LBD cases

The antibody AT8 was used to identify pathologic tau ranging from early aggregates to mature neurofibrillary tangles. The AT8 antibody recognizes tau phosphorylated at serine 202, threonine 205, and serine 208 (pSer202/pThr205/pS208-tau) [28]. In control cases, there was minimal to no immunofluorescence to AT8-tau. In contrast, all of the LBD cases showed immunofluorescence for AT8-tau, as expected from this group with high Braak NFT Stage by design (Fig. 2A). Most immunoreactive tau was neuritic, appearing as short, threadlike inclusions or bright puncta. Occasionally, NFTs were apparent in the soma (Fig. 2B, DLB 2, 6). Overall, the average percent area occupied by AT8-tau was 0.18% (+/- 0.03), and the average for LBD was 13.0% (+/-0.82). Quantification of the percent area occupied by AT8-tau revealed minimal immunoreactivity in control cases with statistically significant increase in abundance of AT8-tau in all LBD cases ($t(7) = 4.5$, $p = 0.003$; Fig. 2B).

MHCII expression in microglia in the middle temporal gyrus of control and LBD cases

Activation and recruitment of immune cells is another pathologic hallmark of LBD [41]. We therefore performed double immunofluorescence for MHCII to identify pro-inflammatory immune cells and Iba1 to identify pro-inflammatory microglia. Control cases showed a small but visible presence of MHCII-pro-inflammatory cells (Fig. 3A). In LBD cases, there was a variable but statistically significant increase in the abundance of pro-inflammatory cells. The average percent area occupied by MHCII was different between control cases (2.6% +/-0.19) and LBD cases (5.9% +/- 0.27; $t(7) = 2.5$, $p = 0.04$; Fig. 3B). There was no difference in the percent area occupied by Iba1 ($t(7) = 0.79$, $p = 0.46$). MHCII colocalized with Iba1 in the merged confocal images. Although there was some MHCII immunoreactivity (green) that did not overlap with Iba1 (magenta), viewing the merged images showed that the MHCII was within the cell boundaries of Iba1, i.e. the MHCII did not colocalize with Iba1 within the same cells. The overlaps of MHCII over Iba1 and Iba1 over MHCII were assessed using Mander's colocalization coefficients. The total overall MHCII fractional overlap over Iba1 was 0.53 (+/- 0.01) in control and 0.52 (+/- 0.01) in LBD cases. Iba1 fractional overlap with MHCII was 0.33 (+/-0.03) for control and 0.48 (+/-0.1) for LBD cases. There were no differences in MHCII/Iba1 colocalization ($t(7) = 0.129$, $p = 0.90$) or Iba1/

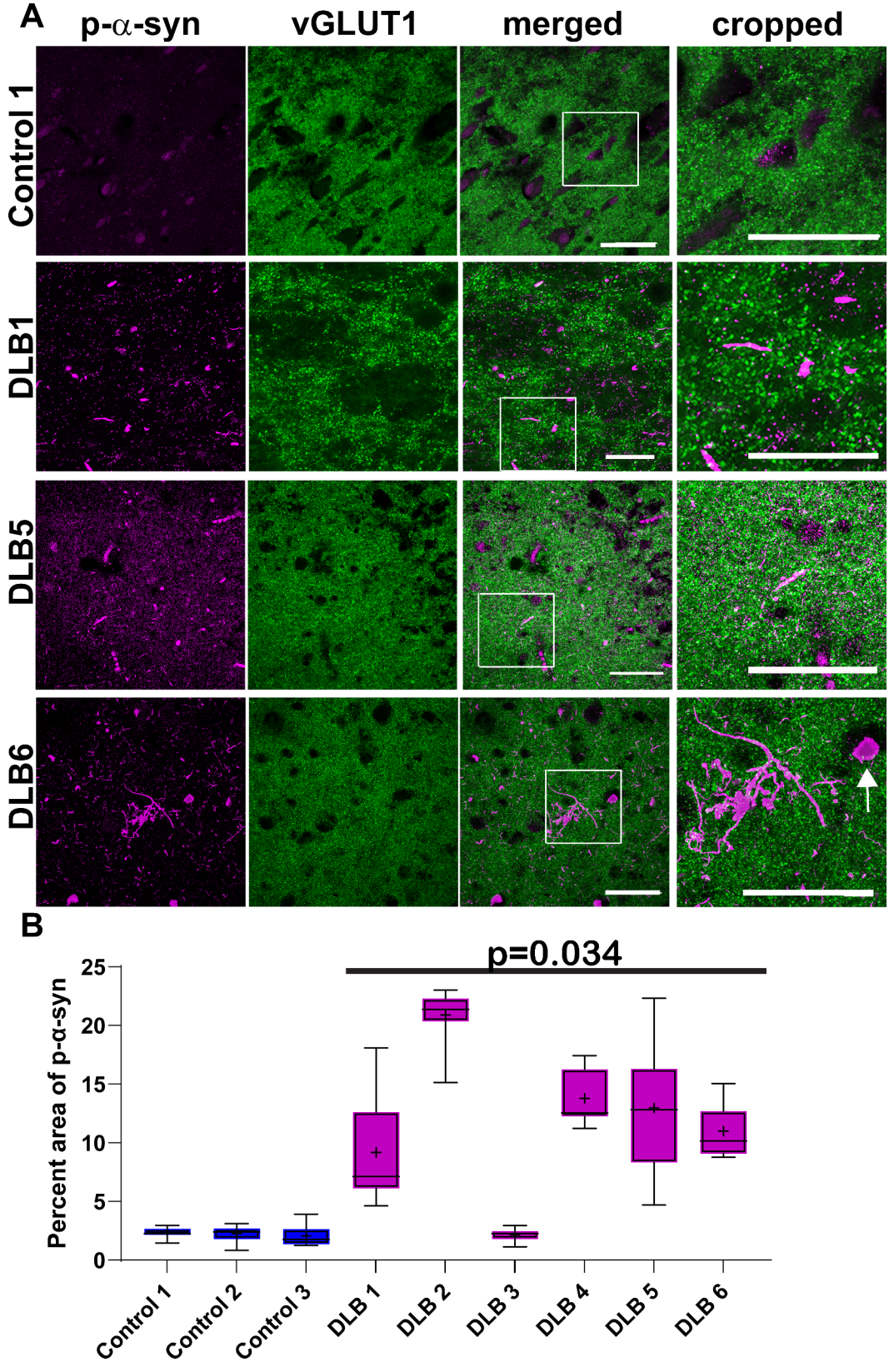

Fig. 1 (See legend on next page.)

(See figure on previous page.)

Fig. 1 **(A)** Immunofluorescence was performed on 40 µm middle temporal cortex sections from three control and six LBD subjects using antibodies to p-α-syn (magenta) and to vGLUT1 (green), a presynaptic marker to allow visualization of the Lewy pathology relative to neuronal synapses. Representative images from one control and three LBD cases are shown. In DLB6, an arrow points to an example of a round p-α-syn aggregate with the morphology of a Lewy body. Scale bar is 50 µm. **(B)** For each control or LBD case, 10 independent confocal frames were analyzed for the percent area occupied by fluorescent signal by a researcher blinded to experimental conditions. Data were analyzed using a mixed effects model with cases as random effect, and control or LBD as fixed effect and image frames as repeated measure. Compound symmetry structure was used for covariance. Data are presented as 5–95% confidence intervals with a "+" indicating the means. $t(7) = 2.6$, $p = 0.034$

MHCII colocalization ($t(7) = 1.88$, $p = 0.1$). Thus, it can be concluded that MHCII is increased in activated microglia in the middle temporal gyrus of LBD cases compared to controls. In addition, the known association between these two proteins and their degree of colocalization sets some expectations for interpreting the following colocalization results between p-α-syn with p-tau.

Analyses of overlap of p-α-syn with p-tau

We then quantified the Mander's colocalization coefficients to determine the extent of overlap of AT8-tau and p-α-syn. Images from temporal cortex incubated with no primary antibodies and the anti-rabbit Alexa Fluor 555 and anti-mouse Alexa Fluor 488 secondary antibodies are shown in Online Resource 2. The majority of p-α-syn immunofluorescence was distinct from AT8-tau immunoreactivity (Fig. 4A). The total overall AT8-tau fractional overlap over p-α-syn was 0.01 (+/- 0.001) in control and 0.03 (+/- 0.002) in LBD groups (Fig. 4B), and there was no difference between groups ($t(7) = 1.0$, $p = 0.35$). When compared to the average 0.53 fractional overall of MHCII over Iba1, two molecules known to colocalize (approximately 0.53, Fig. 3C), the extent of colocalization between AT8-tau and p-α-syn was relatively low. p-α-Syn fractional overlap with AT8-tau was 0.0007 (+/-0.0001) for control and 0.05 (+/-0.005) for LBD cases, and while low, these were significantly different ($t(7) = 4.2$, $p = 0.004$). Areas of overlap could be found. For example, Lewy neurites occasionally were found overlapping with neuritic p-tau (Fig. 4A, top, middle panels). Although dense, circular Lewy bodies were rare, they could be found with p-tau wrapping around them. Thus, p-tau could be found juxtaposed or overlapping with LBD, but the majority of p-α-syn and p-tau appeared distinct.

Analyses of overlap of p-α-syn with PAD-exposed tau

The antibody TNT1 recognizes conformation-dependent exposure of the phosphatase-activating domain (PAD) at the N-terminus of tau [13, 26]. This antibody recognizes early pathologic conformations of tau, and PAD exposure is associated with axonal and synaptic dysfunction [11, 14, 16, 26, 27, 32]. As the majority of p-α-syn localized to neurites in LBD temporal cortex, which is thought to be an earlier form of pathologic α-syn, the overlap of p-α-syn with PAD-exposed tau was analyzed. Control cases showed minimal to no immunoreactivity for PAD-exposed tau when compared to primary delete (Fig. 5A; Online Resource 2). LBD cases showed immunoreactivity for PAD-exposed tau (Fig. 5C). However, the abundance was variable across cases, and there was no difference in the percent area occupied by PAD-exposed tau between LBD and control cases ($t(7) = 1.12$, $p = 0.28$; Fig. 5B). Curiously, the cases with PAD-tau had clinical diagnoses of AD. The fractional overlap of p-α-syn with PAD-exposed tau was 0.026 (+/- 0.03) for controls and 0.024 (+/-0.005) for LBD cases (Fig. 5D), and there was no difference between groups ($t(7) = 0.08$, $p = 0.94$; Fig. 5D). The overlap of PAD-exposed tau and p-α-syn with the fractional overlap for controls was 0.002 (+/- 0.002) and for LBD was 0.074 (+/- 0.02); although small overall, these groups were different ($t(7) = 2.7$, $p = 0.031$). Areas of overlap could be detected in spheroids and Lewy neurites and similar to AT8-tau, the PAD-exposed tau appeared to wrap around or "coat" the p-α-syn.

Discussion

In the present study, we demonstrate three main findings in postmortem human tissue with LBD. First, there is an association of disease markers with the neuropathological diagnosis of LBD, recapitulating that LBD and abnormal tau can contribute to neuronal dysfunction and activate inflammation. Second, early pathologic forms of tau and α-syn rarely co-localize, despite abundant immunoreactivity and the occurrence of both proteins within the same neuronal compartments in some neurons. Third, within neurites and somata, phosphorylated tau and α-syn segregate, where tau is in the outermost part and α-syn in the center of each compartment.

Tau co-pathology often is present in LBD tissue. Prior postmortem studies have reported double-stained neurons for both α-syn and tau [2, 3, 18, 23, 37, 38, 43], and in vitro studies have demonstrated a protein-protein interaction between α-syn and tau [17], suggesting this occurs in LBD patients in a synergistic fashion. In contrast, co-localization is observed in small snapshots, a particular issue for electron microscopy studies in which fewer cells are analyzed and double-labeling with different antibodies is difficult, time-consuming, and subject to selection bias. In contrast, we used several, different immunofluorescent antibodies for phosphorylated tau and α-syn in thick, cortical sections to capture many images over a wide area. We show an abundance of disease and immunologic markers in neuropathologically confirmed cases of LBD yet only rare colocalization

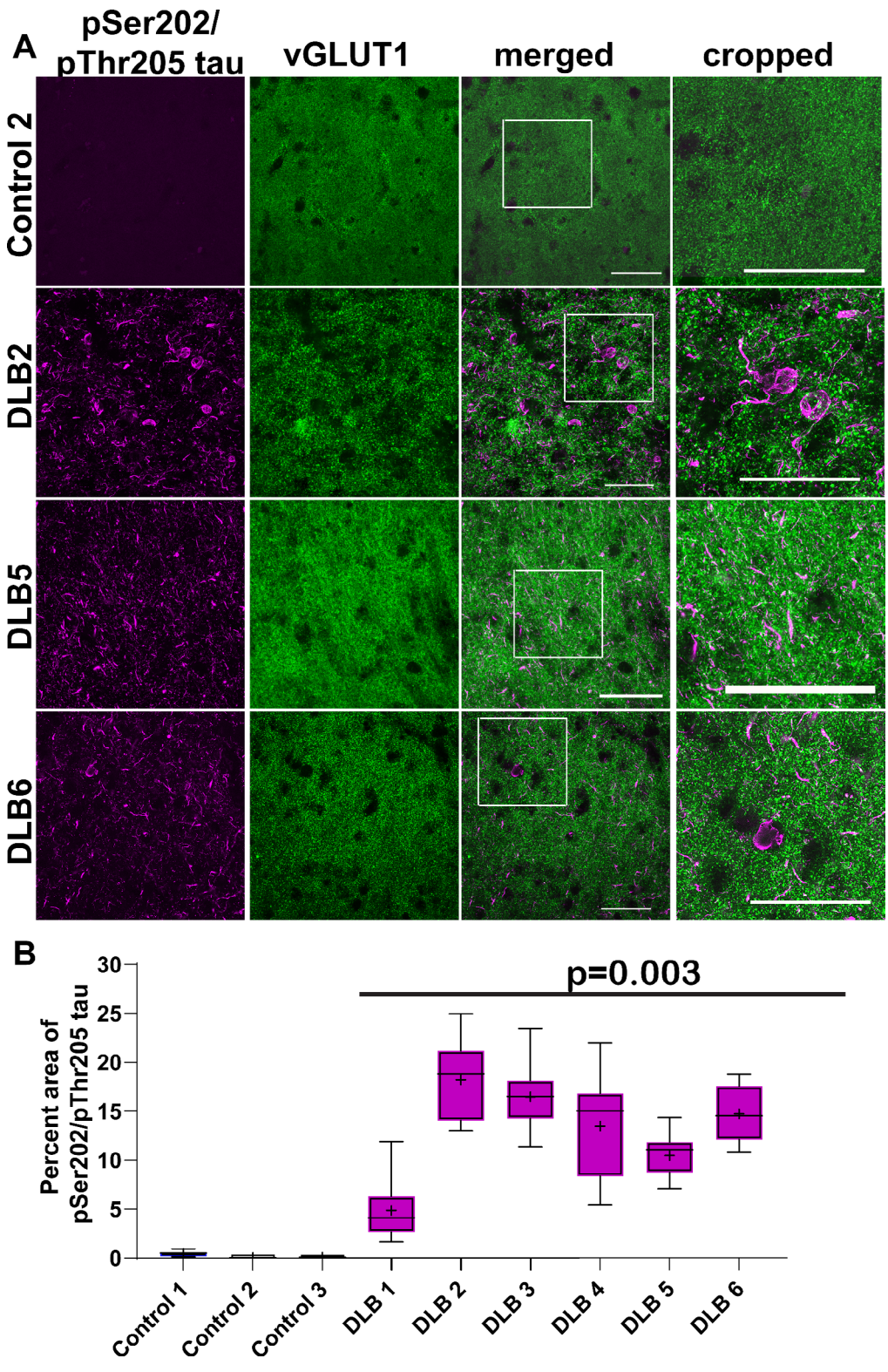

Fig. 2 **(A)** Immunofluorescence was performed on 40 µm temporal cortex sections from three control and six LBD subjects using antibody AT8 to tau pSer202/pThr205 (magenta) and to vGLUT1 (green). Representative images from one control and three LBD cases are shown. Scale bar is 50 µm. **(B)** For each control or LBD case, 10 independent confocal frames were analyzed were analyzed for the percent area occupied by fluorescent signal by a researcher blinded to experimental conditions. Data were analyzed using a mixed effects model with cases as random effect, and control or LBD as fixed effect and image frames as repeated measure. Compound symmetry structure was used for covariance. Data are presented as 5–95% confidence intervals with a "+" indicating the means. $t(7) = 4.5$, $p = 0.003$

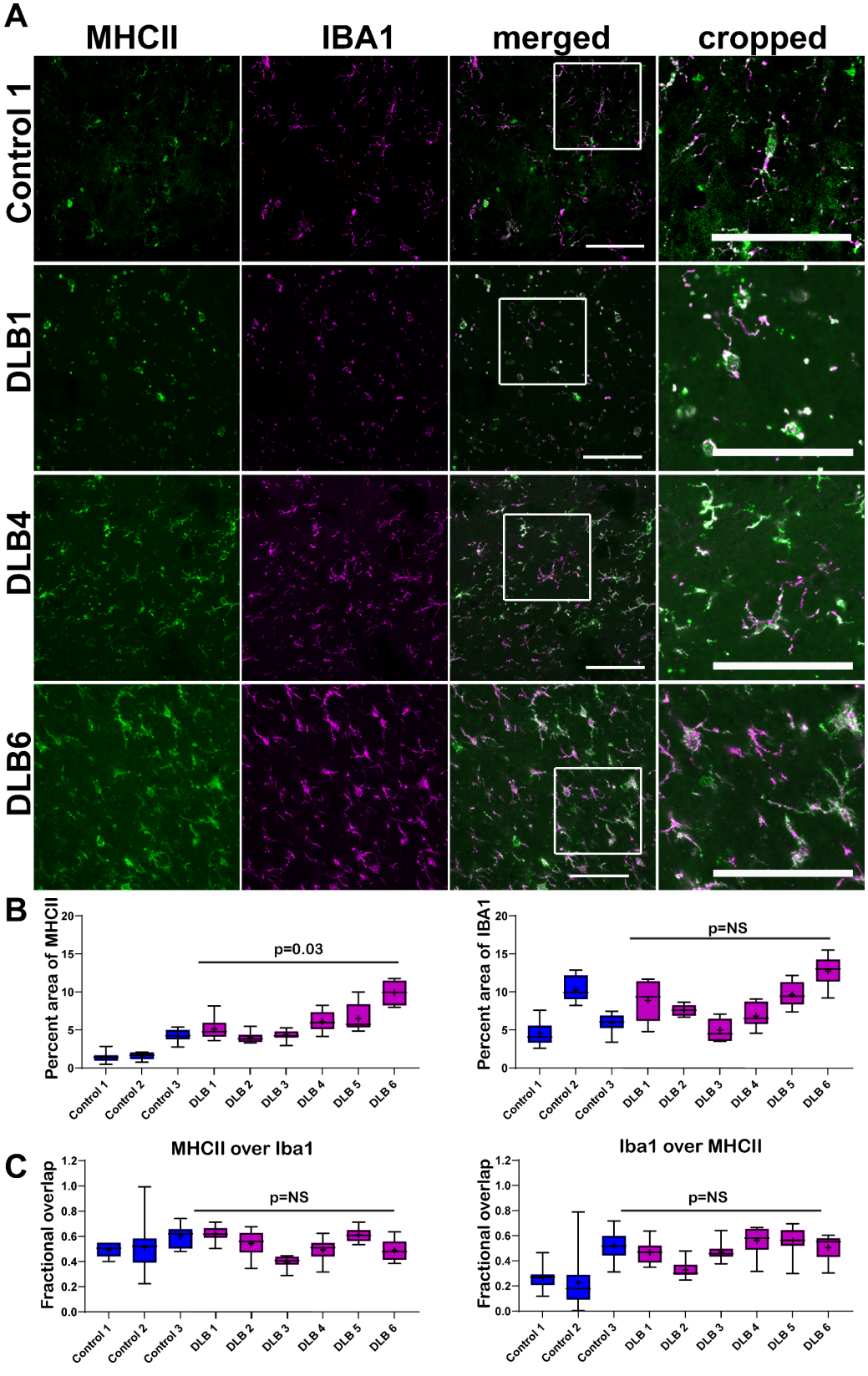

Fig. 3 (See legend on next page.)

(See figure on previous page.)

Fig. 3 **(A)** Immunofluorescence was performed on 40 µm temporal cortex sections from three control and six LBD subjects using antibodies to MHCII (green) and Iba1 (magenta). Representative images from one control and three LBD cases are shown. Scale bar is 50 µm. **(B)** For each control or LBD case, 10 independent confocal frames were analyzed for the percent area occupied by fluorescent signal by a researcher blinded to experimental conditions. Data were analyzed using a mixed effects model with cases as random effect, and control or LBD as fixed effect and image frames as a repeated measure. Compound symmetry structure was used for covariance. Data are presented as 5–95% confidence intervals with a "+" indicating the means. For percent area occupied by MHCII: $t(7) = 2.5$, $p = 0.04$; Iba1: $t(7) = 0.79$, $p = 0.46$. **(C)** Mander's colocalization coefficients were quantified over the 10 independent frames from control and LBD cases to measure fractional overlap of MHCII over Iba1 and Iba1 over MHCII. Data were analyzed using a mixed effects model with cases as random effect, and control or LBD as fixed effect and image frames as a repeated measure. Compound symmetry structure was used for covariance. Data are presented as 5–95% confidence intervals with a "+" indicating the means. For fractional overlap of MHCII over Iba1: $t(7) = 0.129$, $p = 0.90$; For fractional overlap of Iba1 over MHCII, $t(7) = 1.88$, $p = 0.1$

between phosphorylated α-syn and tau. The location of immunoreactive tau and α-syn species primarily was neuritic with few in the soma, and within these compartments, they mostly were segregated when both were present. These results suggest that in temporal cortex, pathologic tau and α-syn deposition are usually independent processes.

The finding that colocalization between phosphorylated α-syn and tau is rare is different from other studies that highlight colocalization between these two proteins. Several factors may help explain this discrepancy. First, many of the antibodies used in prior studies detected all species of α-syn or tau and focused on their co-localization with Lewy bodies; alternatively, the antibodies used in other studies detected oligomeric species, again often with a focus on colocalization with Lewy bodies [2, 3, 18, 23, 37, 38, 43]. Using immunohistochemistry, immunofluorescence, or electron microscopy, tau is detected within Lewy bodies as well as within their peripheral halo, suggesting a deposition hypothesis of an existing aggregate and a later event resulting in another protein depositing on it. However, relatively less is known about colocalization of pre-NFT forms of tau and α-syn within neurites [3, 18, 43]. In the present study, phosphorylated tau is observed in a reticular or circumferential distribution, and phosphorylated α-syn is central; this segregation is seen within the soma and within neurites. Of note, even within the small compartment of a neurite, when both phosphorylated tau and α-syn are present, they still rarely colocalize (but we do not prove no colocalization). It is possible that this reflects a tau/α-syn aggregate core that is inaccessible to antibody labeling, but this is unlikely for the pretangle markers used and the lack of NFT morphology in many of the labeled neurons. We also cannot rule out transient interactions that are indetectable in fixed tissue with confocal microscopy. In addition, proteinase K, which removes normal α-syn, was not included in our immunofluorescence protocol and thus there was p-α-syn in the control tissue, likely resulting in lower p-α-syn/p-tau ratios in the diseased cortex. Future studies using proteinase K could determine if more p-α-syn/p-tau overlap is revealed by this treatment.

Second, regional differences likely change the presence or relative abundance of other proteins that underlie differences in α-syn conformation, its post-translational modifications, its interactions, and ultimately the composition of Lewy bodies or Lewy neurites. This hypothesis is emerging for another neurodegenerative disease [4, 36]. Such differences also may explain the ratio of Lewy bodies to Lewy neurites for an affected brain region. Specific diseases, inflammatory mediators, or mutations may alter the protein folding and aggregation dynamics as well.

Third, selective vulnerability of specific neuronal phenotypes may explain the presence of pathologic tau or α-syn, for example the dopaminergic neurons in the olfactory bulb or substantia nigra versus excitatory neocortical neurons. Within temporal lobe sections pathologic tau and α-syn in adjacent neurons—and sometimes the same neurons—may represent a neuroanatomic convergence of tau-vulnerable and α-syn-vulnerable networks that together result in a worse clinical course [15, 21, 22]. Future studies determining molecular underpinning of differential sensitive of neurons to forming tau aggregates or p-α-syn would be of great interest. Ultimately, how exactly some cases develop more proteinopathies than other cases remains a critical question for understanding heterogeneity in the pathogenesis of neurodegeneration.

There are a few additional limitations that limit the generalizability of these findings. We specifically included LBD cases with a high degree of abnormal tau (namely, only Braak NFT Stages V and VI), and LBD cases without coexisting AD were not examined. As such, it is not known to what degree abnormal tau colocalizes with Lewy bodies and neurites using this method in "pure" LBD cases, though it seems unlikely to be a common phenomenon given the present study's findings. In addition, the total number of cases is relatively small, limiting the confidence in how generalizable the findings are to the population. The cases represented in this study were diverse across clinical diagnoses, and it is known that LBD + AD pathology patients have a lower likelihood of having a DLB clinical phenotype. Indeed, it is common practice to ascribe a major clinical effect for LBD vs. AD [30, 31]. Antemortem diagnosis of LBD is thus difficult to make, especially in the presence of clinical AD [29, 33]. However, the cases in this study were similar in their neuropathogical diagnoses, as assessed

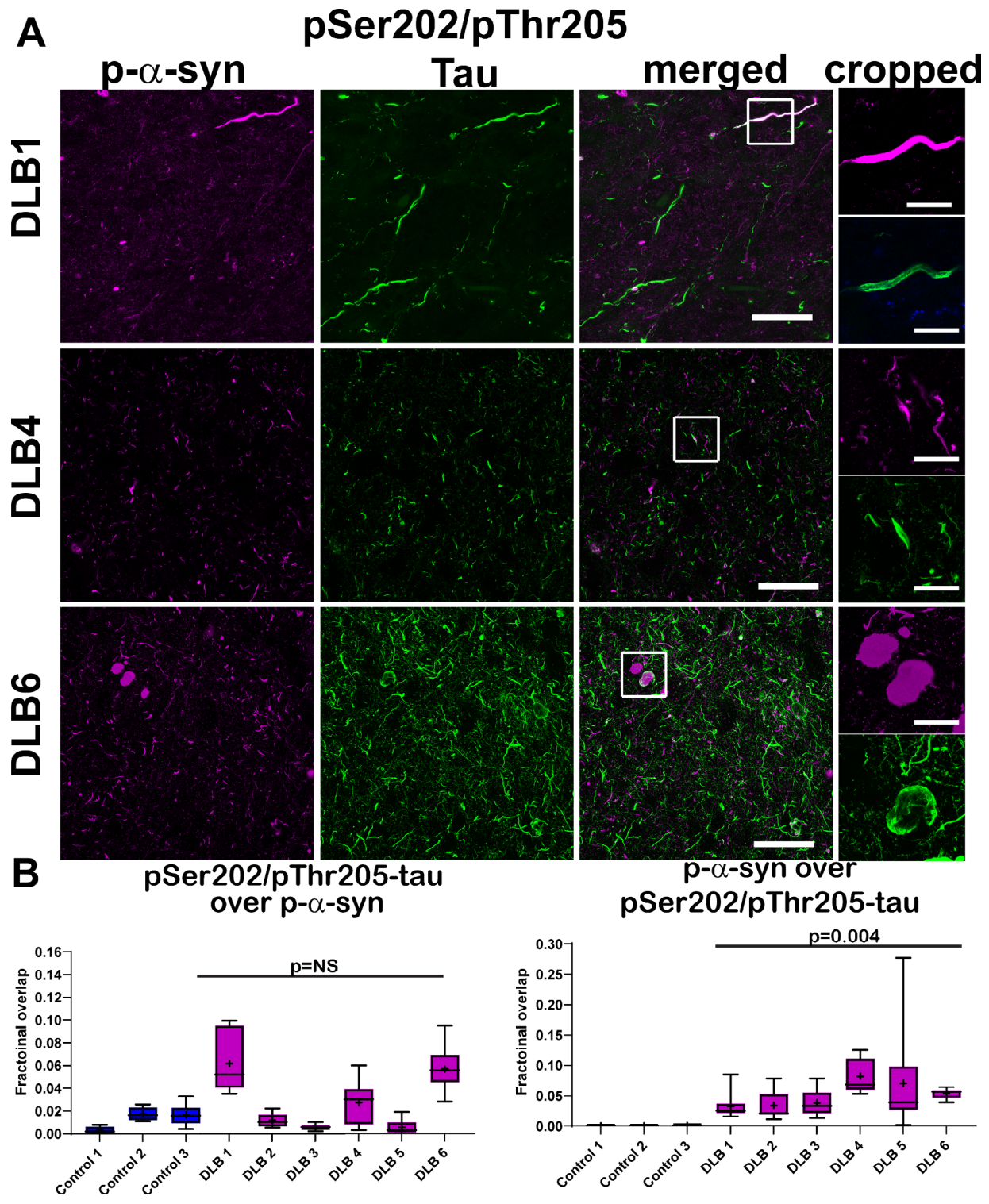

Fig. 4 **(A)** Immunofluorescence was performed on 40 µm temporal cortex sections from three control and six LBD subjects using antibodies to pSer202/pThr205-tau (AT8, green) and p-α-syn (magenta). Representative images from one control and three LBD cases are shown. The cropped images demonstrate that the PAD-exposed tau closely surrounds the p-α-syn, but the two proteins are not coincident. Scale bar is 50 µm–20 µm in cropped images. **(B)** For each control or LBD case, 10 independent confocal frames were analyzed by a researcher blinded to experimental conditions. Data are presented as 5–95% confidence intervals with a "+" indicating the means. Mander's colocalization coefficients were quantified over the 10 independent frames from control and LBD cases to measure fractional overlap of AT8 over p-α-syn and p-α-syn over AT8. Data were analyzed using a mixed effects model with cases as random effect, and control or LBD as fixed effect and image frames as a repeated measure. Compound symmetry structure was used for covariance. For fractional overlap of AT8 over p-α-syn: $t(7) = 1.0$, $p = 0.35$; For fractional overlap of p-α-syn over AT8-tau, $t(7) = 4.2$, $p = 0.004$

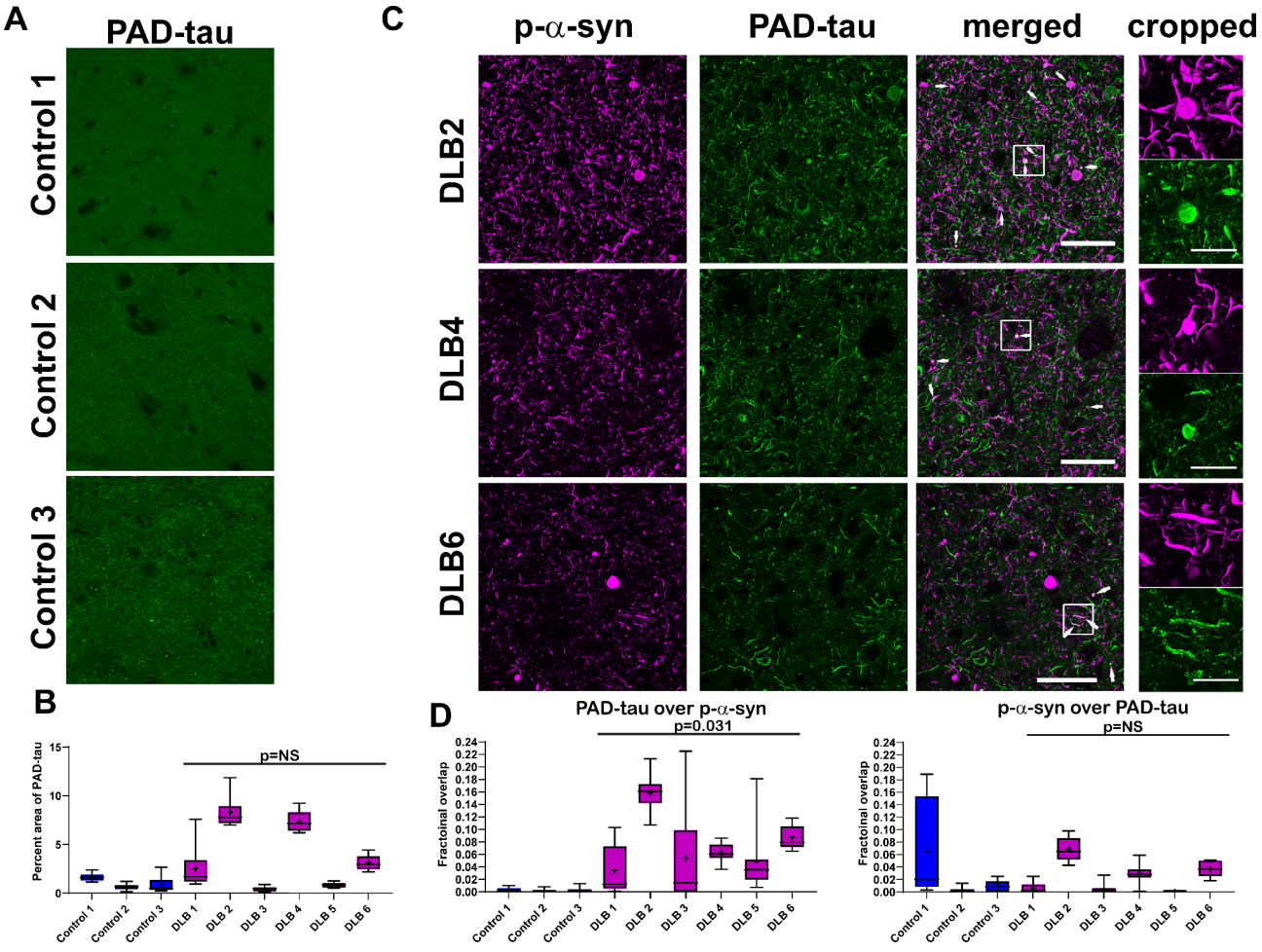

Fig. 5 **(A)** Immunofluorescence was performed on 40 µm temporal cortex sections from three controls and using an antibody to PAD-exposed tau (TNT1, green). Representative images from the three control cases are shown. Scale bar is 50 µm. **(B)** For each case, 10 independent frames were analyzed for the percent area occupied by fluorescent signal. Data are presented as 5–95% confidence intervals with a "+" indicating the means. Data were analyzed using a mixed effects model with cases as random effect, and control or LBD as fixed effect and image frames as a repeated measure. Compound symmetry structure was used for covariance. $t(7) = 1.12$, $p = 0.28$. **(C)** Double labeling immunofluorescence was performed using an antibody to PAD-exposed tau (TNT1, green) and p-α-syn (magenta). Representative images from three LBD cases are shown. Arrows point to areas of proximity of PAD-exposed tau and p-α-syn. The cropped images demonstrate that the PAD-exposed tau closely borders the p-α-syn, but the two proteins do not show total spatial overlap. Scale bar is 50 µm–20 µm in cropped images. **(D)** Mander's colocalization coefficients were quantified over the 10 independent frames from control and LBD cases to measure fractional overlap of PAD-exposed tau over p-α-syn and p-α-syn over PAD-exposed tau. Data are presented as 5–95% confidence intervals with a "+" indicating the means. Data were analyzed using a mixed effects model with cases as random effect, and control or LBD as fixed effect and image frames as a repeated measure. Compound symmetry structure was used for covariance. For fractional overlap of PAD-exposed tau over p-α-syn: $t(7) = 2.7$, $p = 0.031$. For fractional overlap of p-α-syn over PAD-exposed tau: $t(7) = 0.08$, $p = 0.94$

by an expert neuropathologist; although there was variance among clinical diagnoses, there was little variance in abundance of pathology. Lastly, another caveat is that only one region (middle temporal gyrus) was examined, so these findings may vary in different brain regions with different cell types.

In conclusion, phosphorylated α-syn rarely colocalizes with phosphorylated or PAD-exposed tau in temporal lobe sections from LBD postmortem brains. When phosphorylated tau and α-syn were observed in the same neurite or soma, they were segregated within the compartment. The relationship between tau and α-syn co-pathology in LBD is important for explaining clinical symptoms, their severity, and their progression, and researchers should look beyond direct protein-protein interactions for understanding their relationship.

Abbreviations

α-syn	α-synuclein
AD	Alzheimer's disease
DLB	Dementia with Lewy bodies
Iba1	Ionized calcium binding adaptor molecule 1
LBD	Lewy body disease
MHCII	Major-histocompatibility complex class 2
MMSE	Mini-Mental State Exam
NFT	Neurofibrillary tangle

p-	Phosphorylated-
PAD	Phosphatase-activating domain
PD	Parkinson's disease
PDD	Parkinson's disease dementia
SEM	Standard error of the mean
UPDRS	Unified Parkinson's Disease Rating Scale
vGLUT1	Vesicular glutamate transporter 1

Supplementary Information

The online version contains supplementary material available at https://doi.org/10.1186/s40478-024-01913-w.

Online Resource 1. p-α-syn immunofluorescence in Control Case 3 and DLB case 3. The brightness of the images was increased and pseudo-colored black and white to better image the morphology of the p-α-syn. In control cases, small puncta of p-α-syn, likely representing soluble, normal p-α-syn are apparent. Occasionally, cells with diffuse p-α-syn immunofluorescence were visible. In DLB case 3, p-α-syn immunofluorescence was sparse but appeared as Lewy neurites

Online Resource 2. Representative temporal cortical sections, from DLB2 and DLB6, incubated without primary antibody with both anti-rabbit Alexa 555 secondary and anti-mouse IgG1 Alexa 488 secondary. In the main figures cortical sections incubated with an antibody for p-α-syn were then incubated with anti-rabbit Alexa 555 secondary and those incubated with AT8 or TNT1 antibodies were then incubated with anti-mouse Alexa 488 secondary

Acknowledgements
We are grateful to the Banner Sun Health Research Institute Brain and Body Donation Program of Sun City, Arizona for the provision of human brain tissue. Research reported in this publication also was supported by the UAB High Resolution Imaging Facility, the UAB CNET Imaging Core, and the UAB Comprehensive Neuroscience Center Imaging Analysis Core.

Author contributions
This research project was conceived by DLF and LAVD, organized by DLF, GES, TGB, and LAVD, and executed by DLF, MM, OZA, VGC, and LAVD. Statistical analyses were designed and executed by REK and were reviewed by DLF, REK, and LAVD. The manuscript was written first by DLF and LAVD with substantive revisions by DLF, MM, NMK, TGB, and LAVD, and it was reviewed and approved by all authors.

Funding
Financial support was provided by the National Institute of Neurological Disorders and Stroke (NINDS; R56NS117465, R25NS079188). The Banner Sun Health Research Institute Brain and Body Donation Program is supported by the NINDS (U24NS072026 National Brain and Tissue Resource for Parkinson's Disease and Related Disorders), the National Institute on Aging (P30AG019610 and P30AG072980, Arizona Alzheimer's Disease Core Center), the Arizona Department of Health Services (contract 211002, Arizona Alzheimer's Research Center), the Arizona Biomedical Research Commission (contracts 4001, 0011, 05-901, and 1001 to the Arizona Parkinson's Disease Consortium) and the Michael J. Fox Foundation for Parkinson's Research.

Data availability
No datasets were generated or analysed during the current study.

Declarations

Ethics approval and consent to participate
All subjects provided signed informed consents that were ethically approved by designated Banner Sun Health Research Institute Institutional Review Boards.

Consent for publication
Not applicable.

Competing interests
The authors declare no competing interests.

Received: 27 September 2024 / Accepted: 11 December 2024
Published online: 21 January 2025

References

1. Adler CH, Beach TG, Zhang N, Shill HA, Driver-Dunckley E, Caviness JN, Mehta SH, Sabbagh MN, Serrano GE Sue LI (2019) Unified Staging System for Lewy Body Disorders: Clinicopathologic Correlations and Comparison to Braak Staging. J Neuropathol Exp Neurol 78: 891–899 https://doi.org/10.1093/jnen/nlz080
2. Arima K, Hirai S, Sunohara N, Aoto K, Izumiyama Y, Ueda K, Ikeda K, Kawai M (1999) Cellular co-localization of phosphorylated tau- and NACP/alpha-synuclein-epitopes in lewy bodies in sporadic Parkinson's disease and in dementia with Lewy bodies. Brain Res 843:53–61. https://doi.org/10.1016/s0006-8993(99)01848-x
3. Arima K, Mizutani T, Alim MA, Tonozuka-Uehara H, Izumiyama Y, Hirai S, Ueda K (2000) NACP/alpha-synuclein and tau constitute two distinctive subsets of filaments in the same neuronal inclusions in brains from a family of parkinsonism and dementia with Lewy bodies: double-immunolabeling fluorescence and electron microscopic studies. Acta Neuropathol 100:115–121. https://doi.org/10.1007/s004010050002
4. Arseni D, Nonaka T, Jacobsen MH, Murzin AG, Cracco L, Peak-Chew SY, Garringer HJ, Kawakami I, Suzuki H, Onaya M et al (2024) Heteromeric amyloid filaments of ANXA11 and TDP-43 in FTLD-TDP Type C. Nature: https://doi.org/10.1038/s41586-024-08024-5
5. Bates D, Mächler M, Bolker B, Walker S (2015) Fitting Linear Mixed-Effects Models Using lme4. J Stat Softw 67:1–48. https://doi.org/10.18637/jss.v067.i01
6. Beach TG, Adler CH, Sue LI, Serrano G, Shill HA, Walker DG, Lue L, Roher AE, Dugger BN, Maarouf Cet al et al (2015) Arizona Study of Aging and Neurodegenerative Disorders and Brain and Body Donation Program. Neuropathology 35:354–389. https://doi.org/10.1111/neup.12189
7. Beach TG, Serrano GE, Kremer T, Canamero M, Dziadek S, Sade H, Derkinderen P, Corbille AG, Letournel F, Munoz DG et al (2018) Immunohistochemical Method and Histopathology Judging for the Systemic Synuclein Sampling Study (S4). Journal of neuropathology and experimental neurology 77: 793–802 https://doi.org/10.1093/jnen/nly056
8. Bolte S, Cordelieres FP (2006) A guided tour into subcellular colocalization analysis in light microscopy. J Microsc 224:213–232. https://doi.org/10.1111/j.1365-2818.2006.01706.x
9. Brown H, Prescott R (2015) Applied mixed models in medicine. Third edition. edn. John Wiley & Sons Inc., City, pp 1 online resource
10. Cariulo C, Martufi P, Verani M, Azzollini L, Bruni G, Weiss A, Deguire SM, Lashuel HA, Scaricamazza E, Sancesario GM al (2019) Phospho-S129 Alpha-Synuclein Is Present in Human Plasma but Not in Cerebrospinal Fluid as Determined by an Ultrasensitive Immunoassay. Front Neurosci 13:889. https://doi.org/10.3389/fnins.2019.00889
11. Christensen KR, Combs B, Richards C, Grabinski T, Alhadidy MM, Kanaan NM (2023) Phosphomimetics at Ser199/Ser202/Thr205 in Tau Impairs Axonal Transport in Rat Hippocampal Neurons. Mol Neurobiol 60:3423–3438. https://doi.org/10.1007/s12035-023-03281-3
12. Combs B, Kanaan NM (2017) Exposure of the Amino Terminus of Tau Is a Pathological Event in Multiple Tauopathies. Am J Pathol 187:1222–1229. https://doi.org/10.1016/j.ajpath.2017.01.019
13. Combs B, Hamel C, Kanaan NM (2016) Pathological conformations involving the amino terminus of tau occur early in Alzheimer's disease and are differentially detected by monoclonal antibodies. Neurobiol Dis 94:18–31. https://doi.org/10.1016/j.nbd.2016.05.016
14. Combs B, Christensen KR, Richards C, Kneynsberg A, Mueller RL, Morris SL, Morfini GA, Brady ST, Kanaan NM (2021) Frontotemporal Lobar Dementia Mutant Tau Impairs Axonal Transport through a Protein Phosphatase 1gamma-Dependent Mechanism. J neuroscience: official J Soc Neurosci 41:9431–9451. https://doi.org/10.1523/JNEUROSCI.1914-20.2021
15. Coughlin D, Xie SX, Liang M, Williams A, Peterson C, Weintraub D, McMillan CT, Wolk DA, Akhtar RS, Hurtig Hlet al et al (2019) Cognitive and Pathological Influences of Tau Pathology in Lewy Body Disorders. Ann Neurol 85:259–271. https://doi.org/10.1002/ana.25392
16. Cox K, Combs B, Abdelmesih B, Morfini G, Brady ST, Kanaan NM (2016) Analysis of isoform-specific tau aggregates suggests a common toxic mechanism involving similar pathological conformations and axonal transport inhibition.

Neurobiol Aging 47:113–126. https://doi.org/10.1016/j.neurobiolaging.2016.07.015
17. Dasari AKR, Kayed R, Wi S, Lim KH (2019) Tau Interacts with the C-Terminal Region of alpha-Synuclein, Promoting Formation of Toxic Aggregates with Distinct Molecular Conformations. Biochemistry 58:2814–2821. https://doi.org/10.1021/acs.biochem.9b00215
18. Fujishiro H, Tsuboi Y, Lin WL, Uchikado H, Dickson DW (2008) Co-localization of tau and alpha-synuclein in the olfactory bulb in Alzheimer's disease with amygdala Lewy bodies. Acta Neuropathol 116:17–24. https://doi.org/10.1007/s00401-008-0383-1
19. Gerson JE, Farmer KM, Henson N, Castillo-Carranza DL, Carretero Murillo M, Sengupta U, Barrett A, Kayed R (2018) Tau oligomers mediate alpha-synuclein toxicity and can be targeted by immunotherapy. Mol neurodegeneration 13:13. https://doi.org/10.1186/s13024-018-0245-9
20. Giasson BI, Forman MS, Higuchi M, Golbe LI, Graves CL, Kotzbauer PT, Trojanowski JQ, Lee VM (2003) Initiation and synergistic fibrillization of tau and alpha-synuclein. Science 300:636–640. https://doi.org/10.1126/science.1082324
21. Irwin DJ, White MT, Toledo JB, Xie SX, Robinson JL, Van Deerlin V, Lee VM, Leverenz JB, Montine TJ, Duda JEet al et al (2012) Neuropathologic substrates of Parkinson disease dementia. Ann Neurol 72:587–598. https://doi.org/10.1002/ana.23659
22. Irwin DJ, Grossman M, Weintraub D, Hurtig HI, Duda JE, Xie SX, Lee EB, Van Deerlin VM, Lopez OL, Kofler JK al (2017) Neuropathological and genetic correlates of survival and dementia onset in synucleinopathies: a retrospective analysis. Lancet Neurol 16:55–65. https://doi.org/10.1016/S1474-4422(16)30291-5
23. Iseki E, Marui W, Kosaka K, Ueda K (1999) Frequent coexistence of Lewy bodies and neurofibrillary tangles in the same neurons of patients with diffuse Lewy body disease. Neurosci Lett 265:9–12. https://doi.org/10.1016/s0304-3940(99)00178-0
24. Iseki E, Takayama N, Marui W, Ueda K, Kosaka K (2002) Relationship in the formation process between neurofibrillary tangles and Lewy bodies in the hippocampus of dementia with Lewy bodies brains. J Neurol Sci 195:85–91. https://doi.org/10.1016/s0022-510x(01)00689-x
25. Ishizawa T, Mattila P, Davies P, Wang D, Dickson DW (2003) Colocalization of tau and alpha-synuclein epitopes in Lewy bodies. J Neuropathol Exp Neurol 62:389–397. https://doi.org/10.1093/jnen/62.4.389
26. Kanaan NM, Morfini GA, LaPointe NE, Pigino GF, Patterson KR, Song Y, Andreadis A, Fu Y, Brady ST, Binder LI (2011) Pathogenic forms of tau inhibit kinesin-dependent axonal transport through a mechanism involving activation of axonal phosphotransferases. J neuroscience: official J Soc Neurosci 31:9858–9868. https://doi.org/10.1523/JNEUROSCI.0560-11.2011
27. Kanaan NM, Morfini G, Pigino G, LaPointe NE, Andreadis A, Song Y, Leitman E, Binder LI, Brady ST (2012) Phosphorylation in the amino terminus of tau prevents inhibition of anterograde axonal transport. Neurobiology of aging 33: 826 e815-830 https://doi.org/10.1016/j.neurobiolaging.2011.06.006
28. Malia TJ, Teplyakov A, Ernst R, Wu SJ, Lacy ER, Liu X, Vandermeeren M, Mercken M, Luo J, Sweet RW et al (2016) Epitope mapping and structural basis for the recognition of phosphorylated tau by the anti-tau antibody AT8. Proteins 84: 427–434 https://doi.org/10.1002/prot.24988
29. McKeith I, Taylor JP, Thomas A, Donaghy P, Kane J (2016) Revisiting DLB Diagnosis: A Consideration of Prodromal DLB and of the Diagnostic Overlap With Alzheimer Disease. J Geriatr Psychiatry Neurol 29:249–253. https://doi.org/10.1177/0891988716656083
30. McKeith IG, Boeve BF, Dickson DW, Halliday G, Taylor JP, Weintraub D, Aarsland D, Galvin J, Attems J, Ballard CG et al (2017) Diagnosis and management of dementia with Lewy bodies: Fourth consensus report of the DLB Consortium. Neurology 89: 88–100 https://doi.org/10.1212/WNL.0000000000004058
31. Montine TJ, Phelps CH, Beach TG, Bigio EH, Cairns NJ, Dickson DW, Duyckaerts C, Frosch MP, Masliah E, Mirra SSet al et al (2012) National Institute on Aging-Alzheimer's Association guidelines for the neuropathologic assessment of Alzheimer's disease: a practical approach. Acta Neuropathol 123:1–11. https://doi.org/10.1007/s00401-011-0910-3
32. Moreno H, Morfini G, Buitrago L, Ujlaki G, Choi S, Yu E, Moreira JE, Avila J, Brady ST, Pant Het al et al (2016) Tau pathology-mediated presynaptic dysfunction. Neuroscience 325:30–38. https://doi.org/10.1016/j.neuroscience.2016.03.044
33. Nelson PT, Jicha GA, Kryscio RJ, Abner EL, Schmitt FA, Cooper G, Xu LO, Smith CD, Markesbery WR (2010) Low sensitivity in clinical diagnoses of dementia with Lewy bodies. J Neurol 257:359–366. https://doi.org/10.1007/s00415-009-5324-y
34. Parra-Rivas LA, Madhivanan K, Aulston BD, Wang L, Prakashchand DD, Boyer NP, Saia-Cereda VM, Branes-Guerrero K, Pizzo DP, Bagchi Pet al et al (2023) Serine-129 phosphorylation of alpha-synuclein is an activity-dependent trigger for physiologic protein-protein interactions and synaptic function. Neuron 111: 4006–4023 e4010 https://doi.org/10.1016/j.neuron.2023.11.020
35. Ramalingam N, Jin SX, Moors TE, Fonseca-Ornelas L, Shimanaka K, Lei S, Cam HP, Watson AH, Brontesi L, Ding Let al et al (2023) Dynamic physiological alpha-synuclein S129 phosphorylation is driven by neuronal activity. NPJ Parkinsons Dis 9(4). https://doi.org/10.1038/s41531-023-00444-w
36. Robinson JL, Suh E, Xu Y, Hurtig HI, Elman L, McMillan CT, Irwin DJ, Porta S, Van Deerlin VM, Lee EB (2024) Annexin A11 aggregation in FTLD-TDP type C and related neurodegenerative disease proteinopathies. Acta Neuropathol 147:104. https://doi.org/10.1007/s00401-024-02753-7
37. Schmidt ML, Martin JA, Lee VM, Trojanowski JQ (1996) Convergence of Lewy bodies and neurofibrillary tangles in amygdala neurons of Alzheimer's disease and Lewy body disorders. Acta Neuropathol 91:475–481. https://doi.org/10.1007/s004010050454
38. Sengupta U, Guerrero-Munoz MJ, Castillo-Carranza DL, Lasagna-Reeves CA, Gerson JE, Paulucci-Holthauzen AA, Krishnamurthy S, Farhed M, Jackson GR, Kayed R (2015) Pathological interface between oligomeric alpha-synuclein and tau in synucleinopathies. Biol Psychiatry 78:672–683. https://doi.org/10.1016/j.biopsych.2014.12.019
39. Singh B, Covelo A, Martell-Martinez H, Nanclares C, Sherman MA, Okematti E, Meints J, Teravskis PJ, Gallardo C, Savonenko AV al (2019) Tau is required for progressive synaptic and memory deficits in a transgenic mouse model of alpha-synucleinopathy. Acta Neuropathol 138:551–574. https://doi.org/10.1007/s00401-019-02032-w
40. Spina S, La Joie R, Petersen C, Nolan AL, Cuevas D, Cosme C, Hepker M, Hwang JH, Miller ZA, Huang EJ al (2021) Comorbid neuropathological diagnoses in early versus late-onset Alzheimer's disease. Brain 144:2186–2198. https://doi.org/10.1093/brain/awab099
41. Standaert DG, Harms AS, Childers GM, Webster JM (2023) Disease mechanisms as subtypes: Inflammation in Parkinson disease and related disorders. Handb Clin Neurol 193:95–106. https://doi.org/10.1016/B978-0-323-85555-6.00011-4
42. Stoyka LE, Mahoney CL, Thrasher DR, Russell DL, Cook AK, Harris AT, Narayanan A, Janado TP, Standaert DG, Roberson ED et al (2021) Templated alpha-Synuclein Inclusion Formation Is Independent of Endogenous Tau. eNeuro 8: https://doi.org/10.1523/ENEURO.0458-20.2021
43. Uchikado H, Lin WL, DeLucia MW, Dickson DW (2006) Alzheimer disease with amygdala Lewy bodies: a distinct form of alpha-synucleinopathy. J Neuropathol Exp Neurol 65:685–697. https://doi.org/10.1097/01.jnen.0000225908.90052.07

Publisher's note